

Neutral bis(1,4-diaza-1,3-butadiene)nickel complexes and their corresponding monocations: molecular and electronic structures. A combined experimental and density functional theoretical study†‡

Nicoleta Muresan, Thomas Weyhermüller and Karl Wieghardt*

Received 20th June 2007, Accepted 23rd August 2007

First published as an Advance Article on the web 10th September 2007

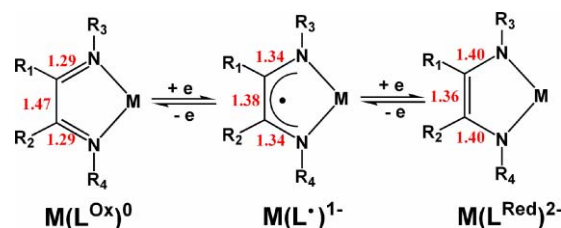
DOI: 10.1039/b709390j

The reaction of 2 equivalents of 2-methyl-1,4-bis(2,6-dimethylphenyl)-1,4-diaza-1,3-butadiene, (${}^1L^{Ox}$) 0 , or 2-methyl-1,4-bis(2,6-diisopropylphenyl)-1,4-diaza-1,3-butadiene, (${}^2L^{Ox}$) 0 , in diethyl ether or *n*-hexane with 1 equivalent of Ni(cdt) where (cdt) 0 is the ligand cyclododecatriene affords dark red, diamagnetic precipitates of [Ni^{II}(1L) $_2$] (**1**) and of [Ni^{II}(2L) $_2$] (**3**). The ligands (1L) $^{1-}$ and (2L) $^{1-}$ are the one-electron reduced, monoanionic π radicals of the above neutral 1,4-diaza-1,3-butadienes. **1** and **3** have been structurally characterized by X-ray crystallography; both possess a distorted tetrahedral geometry where the dihedral angle θ between the two metallacycles Ni–N–C–C–N is 47.9° and 53°, respectively, ($\theta = 0^\circ$ for square planar and 90° for a regular tetrahedral geometry). The reaction of **1** and **3** with 1 equivalent of ferrocenium hexafluorophosphate gives the paramagnetic ($S_t = 1/2$) complexes **2** and **4**, respectively: [Ni^I(${}^1L^{Ox}$) $_2$](PF $_6$) (**2**), [Ni^I(${}^2L^{Ox}$) $_2$](PF $_6$) (**4**). Their EPR spectra indicate the presence of a central Ni(I) ion (d^9 ; $S_{Ni} = 1/2$). Thus, the one-electron *oxidation* of **1** and **3** by [Fc]PF $_6$ induces an intramolecular one-electron *reduction* of the central Ni ion and a concomitant one-electron *oxidation* of the second π radical ($L^{\cdot-} \rightarrow L^{Ox} + e$). Broken symmetry DFT calculations (B3LYP) corroborate the correctness of the electronic structure descriptions of **1–4**. The reaction of (${}^1L^{Ox}$) 0 with NiI $_2$ (1 : 1) in tetrahydrofuran yields tetrahedral [Ni^{III}(${}^1L^{Ox}$) $_2$] (**5**) with an $S_t = 1$ ground state.

Introduction

It has now been clearly established by spectroscopy and X-ray crystallography as well as density functional theoretical calculations that neutral, distorted tetrahedral bis(1,4-diaza-1,3-butadiene)nickel complexes^{1–6} possess an electronic structure which is best described as nickel(II) species (d^8 ; $S_{Ni} = 1$) containing two monoanionic π radical ligands.^{5–7} The two singly occupied metal d-orbitals (t_2 in T_d symmetry) are coupled intramolecularly antiferromagnetically to two ligand π radicals ($S_{rad} = 1/2$) yielding a diamagnetic ground state ($S_t = 0$):^{5–7} [Ni^{II}($L^{\cdot-}$) $_2$]. It has been shown by DFT calculations that these neutral 1,4-diaza-1,3-butadiene ligands possess an empty energetically low-lying, antibonding π^* orbital^{8–10} (with respect to the C–N bond but *bonding* with respect to the C–C bond) which readily accepts one-electron generating a monoanionic π radical, ($L^{\cdot-}$) $^{1-}$, or two electrons affording a closed-shell enediamide (L^{Red}) $^{2-}$ as shown in Scheme 1.

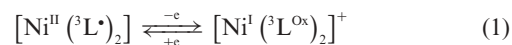
Balch and Holm¹ have demonstrated as early as 1966 that these neutral nickel complexes, [Ni(L) $_2$] z , are a member of one respective electron transfer series where $z = 0, 1-, 2-,$ and $1+, 2+$. We have recently discovered for the species [Ni^{II}(3L) $_2$] ($S = 0$) (Chart I) that its one-electron oxidation leads to the tetrahedral monocation



Scheme 1

[Ni^I(${}^3L^{Ox}$) $_2$] $^+$ ($S = 1/2$) with a central nickel(I) ion (d^9) and two neutral, closed-shell (${}^3L^{Ox}$) 0 ligands.⁶

One might envisage reaction (1) as an oxidatively induced reduction of the metal center or, conversely, a reductively induced oxidation of the central metal ion.



In order to test the generality of this reaction we have synthesized two new neutral complexes, **1** and **3**, and oxidized them with one equivalent of ferrocenium hexafluorophosphate to the corresponding monocations in **2** and **4** (Chart 1). We have also synthesized and characterized the neutral complex [Ni^{III}(${}^1L^{Ox}$) $_2$] (**5**) which possesses an $S_t = 1$ ground state.

Complexes **1** and **3** differ in the steric bulkiness of the N,N'-substituents when N,N'-coordinated in the bis(ligand)nickel complexes. Consequently, the dihedral angle θ between the two five-membered chelate rings Ni–N–C–C–N varies from $\sim 40^\circ$ to 90° (θ is 0° in a square planar complex and 90° in a regular tetrahedral species). Thus, the present study was initiated to explore the influence of θ on the electronic structure of these complexes.

Max-Planck-Institut für Bioorganische Chemie, Stiftstrasse 34-36, D-45470, Mülheim an der Ruhr, Germany

† CCDC reference numbers 650249–650251. For crystallographic data in CIF or other electronic format see DOI: 10.1039/b709390j

‡ Electronic supplementary information (ESI) available: Optimized geometries, spin density maps and qualitative MO schemes for the complexes. See DOI: 10.1039/b709390j

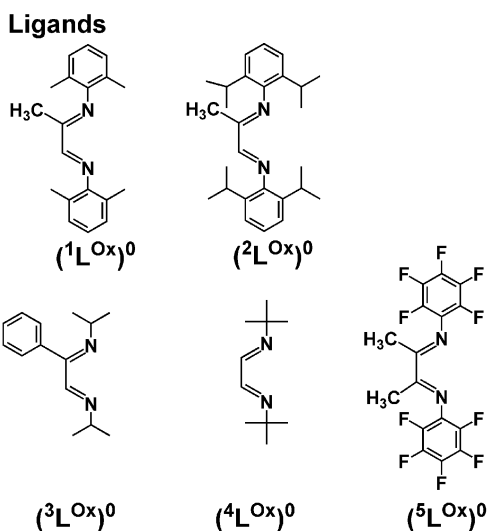
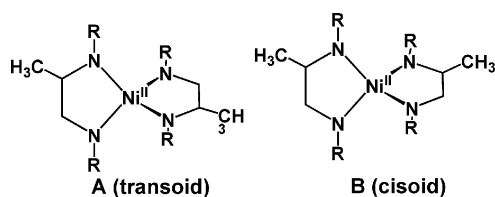


Chart 1

Note that the ligands (${}^1\text{L}^{\text{Ox}})^0$ and (${}^2\text{L}^{\text{Ox}})^0$ carry a single methyl group at the 1,4-diaza-1,3-butadiene backbone in the 2-position. This, in principle, induces an asymmetry which leads to the existence of two geometrical isomers^{6,11} of distorted tetrahedral complexes containing two such bidentate ligands provided that the dihedral angle θ between the two five-membered chelate rings is $\neq 90^\circ$. In this case the two diastereomers **A** and **B** prevail.



The coordination chemistry of N,N'-disubstituted α -diimines with main group metal ions (Li, Mg, Al, Ga, In) and zinc(II) ions has been investigated in detail experimentally and theoretically.^{12–25} It has been shown—mainly by X-ray crystallography—that these ligands can adopt three different oxidation levels, namely the neutral α -diimines, ($\text{L}^{\text{Ox}})^0$, monoanionic π radicals, (L^\bullet)^{1–}, and the reduced α -diamides (L^{Red})^{2–} as displayed in Scheme 1. They clearly differ in their respective C–N and C–C bond lengths.

Results and discussion

Syntheses and spectroscopic characterizations

The reaction of 1 equivalent of $[\text{Ni}(\text{cdt})]^\circ$ (cdt = cyclododecatriene) with 2 equivalents of the N,N'-disubstituted 1,4-diaza-

1,3-butadiene ligands (${}^1\text{L}^{\text{Ox}})^0$ and (${}^2\text{L}^{\text{Ox}})^0$ shown in Chart 1 in diethyl ether or an *n*-hexane–diethyl ether mixture (1 : 1 v/v) at ambient temperature affords dark red precipitates of the neutral complexes $[\text{Ni}^{\text{II}}(\text{}^1\text{L}^\bullet)_2]$ (**1**) and $[\text{Ni}^{\text{II}}(\text{}^2\text{L}^\bullet)_2]\cdot\text{hexane}$ (**3**) in $\sim 80\%$ yield, respectively. Both species are quite air-sensitive.

Oxidation of **1** and **3** in CH_2Cl_2 at 20°C with 1 equivalent of ferrocenium hexafluorophosphate, $[\text{Fc}](\text{PF}_6)$, affords dark violet microcrystals of $[\text{Ni}^{\text{II}}(\text{}^1\text{L}^{\text{Ox}})_2](\text{PF}_6)$ (**2**) and $[\text{Ni}^{\text{II}}(\text{}^2\text{L}^{\text{Ox}})_2](\text{PF}_6)$ (**4**) in $\sim 90\%$ yield.

Finally, the reaction of NiI_2 in tetrahydrofuran with 1 equivalent of the ligand (${}^1\text{L}^{\text{Ox}})^0$ gives red $[\text{Ni}^{\text{II}}(\text{}^1\text{L}^{\text{Ox}})_2\text{I}_2]$ (**5**) in $\sim 90\%$ yield.

Complexes **1** and **3** are diamagnetic as was judged from their “normal” ${}^1\text{H}$ NMR spectra (see below and Experimental section); they possess an $S_{\text{t}} = 0$ ground state. In contrast, complexes **2** and **4** are paramagnetic. From temperature-dependent magnetic susceptibility measurements (4–300 K) temperature-independent magnetic moments of $1.9 \mu_{\text{B}}$ and $1.88 \mu_{\text{B}}$, respectively, have been measured. Thus, both **2** and **4** possess an $S = 1/2$ ground state. As expected, a magnetic moment of $2.9 \mu_{\text{B}}$ for **5** indicates an $S = 1$ ground state.

The cyclic voltammogram of **1** in tetrahydrofuran solution (0.10 M $[\text{N}(\text{n-Bu})_4]\text{PF}_6$) measured at 20°C at a glassy carbon working electrode is shown in Fig. 1. Ferrocene was used as internal standard, and potentials are referenced vs. the ferrocenium–ferrocene couple (Fc^+/Fc). The cyclic voltammogram of **2** is identical to that of **1** shown in Fig. 1.

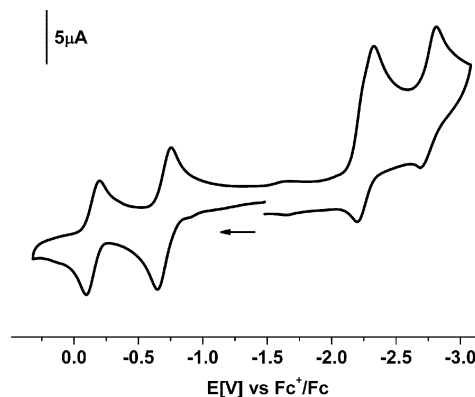
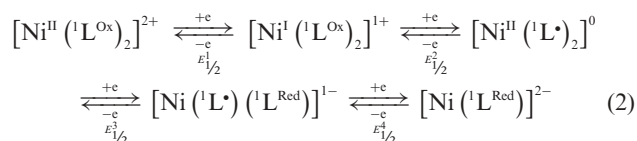


Fig. 1 Cyclic voltammogram of **1** in tetrahydrofuran (0.10 M $[\text{N}(\text{n-Bu})_4]\text{PF}_6$ supporting electrolyte) at 20°C at a glassy carbon working electrode.

Four reversible one-electron transfer waves have been observed at $E_{1/2}^1 = -0.16 \text{ V}$, $E_{1/2}^2 = -0.70 \text{ V}$, $E_{1/2}^3 = -2.25 \text{ V}$, and $E_{1/2}^4 = -2.80 \text{ V}$ vs. Fc^+/Fc ; the first two correspond to two successive one-electron oxidations of **1** whereas the latter two are one-electron reductions as shown by coulometry at appropriately fixed potentials, eqn (2).



Interestingly, the cyclic voltammogram of **3** (or **4**) in THF at 20°C displays only two oxidation waves: $E_{\text{p,c}}^1 = -1.4$, $E_{\text{p,a}} = -0.8$ ($E_{1/2}$ ca. -1.1 V) and $E_{1/2}^2 = -0.5 \text{ V}$ (reversible) Fc^+/Fc in the range -1.6 V to 0.0 V .

The electronic spectra of the neutral complexes **1** and of the monocation in **2** in CH_2Cl_2 solution at 20°C are displayed in Fig. 2 (top); those of the corresponding species **3** and **4** are also shown (bottom). The spectrum of **5** in CH_2Cl_2 is shown in Fig. 3. Table 1 summarizes the data.

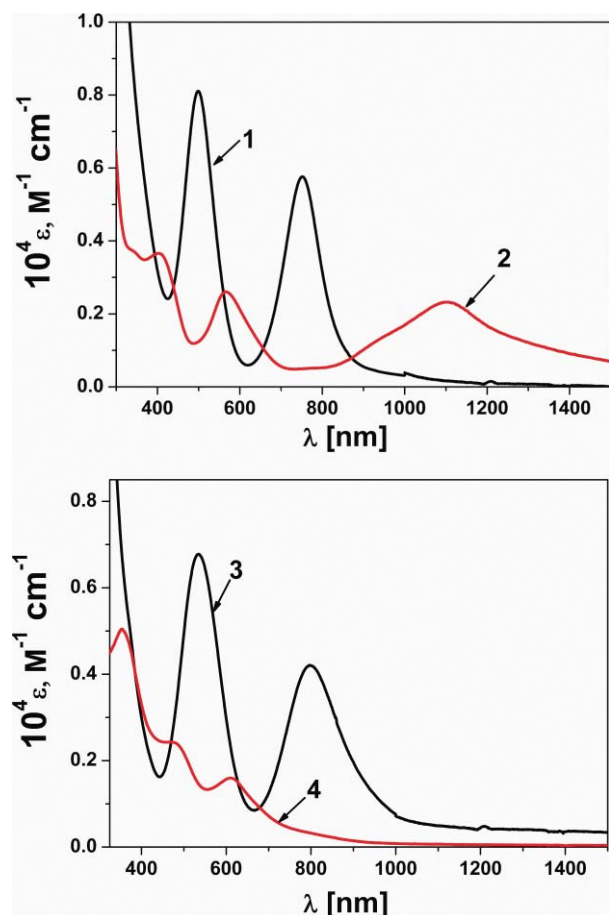


Fig. 2 Electronic spectra of **1** and **2** (top) and **3** and **4** (bottom) in CH_2Cl_2 solution at 20°C .

The electronic spectra of all neutral complexes $[\text{Ni}^{\text{II}}(\text{L}^*)_2]$ are very similar.² They consist of an intense absorption maximum at $\sim 500 \pm 50$ nm with an extinction coefficient $\epsilon \sim 10^4 \text{ M}^{-1} \text{ cm}^{-1}$ and a second absorption maximum in the near infrared at $750 \pm$

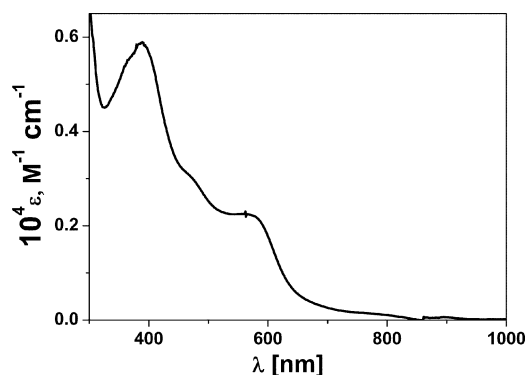


Fig. 3 Electronic spectrum of **5** in CH_2Cl_2 solution at 20°C .

Table 1 Electronic spectra of complexes in CH_2Cl_2 solution

Complex	λ/nm ($10^4 \epsilon/\text{M}^{-1} \text{ cm}^{-1}$)
1	497 (0.8), 751 (0.6)
2	404 (0.4), 567 (0.3), 1100 (0.2)
3	531 (0.3), 789 (0.2)
4	360 (0.5), 478 (0.2), 610 (0.2)
5	388 (0.6), 472 (0.3) sh, 578 (0.22)
$[\text{Ni}^{\text{II}}(\text{L}^*)_2]^a$	495 (1.5), 700 (0.09)
$[\text{Ni}^{\text{I}}(\text{L}^{\text{ox}})]^{+a}$	559 (0.9), 610 sh, 757 (0.4) sh, 1700 (0.2)

^a Ref. 6.

100 nm. The intensity of this transition appears to correlate with the dihedral angle θ (between the two five-membered chelate rings) of these neutral complexes as shown in Table 2 and Fig. 4 where a plot of $\log \epsilon$ vs. θ is linear ($R = 0.982$). Interestingly, in square planar complexes⁹ ($\theta = 0^\circ$) this transition exhibits an intensity of $\epsilon \sim 5 \times 10^4 \text{ M}^{-1} \text{ cm}^{-1}$ whereas in nearly regular tetrahedral complexes ($\theta = 88.3^\circ$)^{2b} ϵ is small at $\sim 350 \text{ M}^{-1} \text{ cm}^{-1}$.

In ref.9 this transition has been identified for square planar complexes as ligand-to-ligand charge transfer (LLCT) rather than a simple HOMO–LUMO transition. In square planar complexes this transition is dipole- and spin-allowed. It carries a significant amount of information about the very large ground state exchange coupling.⁹ In tetrahedral complexes of this type the LLCT transition is spin-forbidden and, thus, its intensity is significantly decreased (Scheme 2).

The X-band EPR spectra of **2** and **4** have been recorded in a CH_2Cl_2 –toluene mixture and CH_2Cl_2 at 30 and 10 K, respectively;

Table 2 Correlation between the dihedral angle θ and $\log \epsilon$ of the lowest-energy transition in the near infrared spectrum^a

Complex	No. ^b	Ref.	$\theta/^\circ$	$\lambda_{\text{max}}/\text{nm}$	$\epsilon^\text{c}/\text{L mol}^{-1} \text{ cm}^{-1}$	$\log \epsilon$
1	1	This work	47.9	751	0.58×10^4	3.76
3	2	This work	53	789	0.20×10^4	3.30
$[\text{Ni}^{\text{II}}(\text{L}^*)_2]^0$	3	6	78.9	700	0.9×10^3	2.95
$[\text{Ni}^{\text{II}}(\text{L}^*)_2]^0$	4	5	55.3	756	3.20×10^3	3.50
$[\text{Ni}^{\text{II}}(\text{L}^*)_2]^0$	5	9	0	790	5.43×10^4	4.73
$[\text{Ni}^{\text{II}}(\text{L}^*)_2]^0$	6	9	0	839	4.0×10^4	4.60
$[\text{Ni}^{\text{II}}(\text{L}^*)_2]^0$	7	4(b)	51	768	0.5×10^4	3.70
$[\text{Ni}^{\text{II}}(\text{L}^*)_2]^0$	8	2(b)	88.3	682	0.035×10^4	2.54
$[\text{Ni}^{\text{II}}(\text{L}^*)_2]^0$	9	2(c)	44.5	732	0.66×10^4	3.82

^a Ligand abbreviations: $(\text{L}^{\text{Red}})^{2-} = 3,5\text{-di-}i\text{-tert-butyl-}o\text{-phenylenediimide}(2-)$; $(\text{L}^{\text{Red}})^{2-} = N\text{-phenyl-}o\text{-phenylenediimide}(2-)$; $(\text{L}^{\text{Ox}})^0 = N,N'\text{-bis}(2,6\text{-isopropylphenyl})\text{-1,4-diaza-1,3-butadiene}$; $(\text{L}^{\text{Ox}})^0 = N,N'\text{-bis}(\text{cyclohexyl})\text{-1,4-diaza-1,3-butadiene}$; $(\text{L}^{\text{Ox}})^0 = N,N'\text{-bis}(2,6\text{-dimethylphenyl})\text{-1,4-diaza-1,3-butadiene}$. ^b Number of complex in Fig. 4. ^c Extinction coefficient.

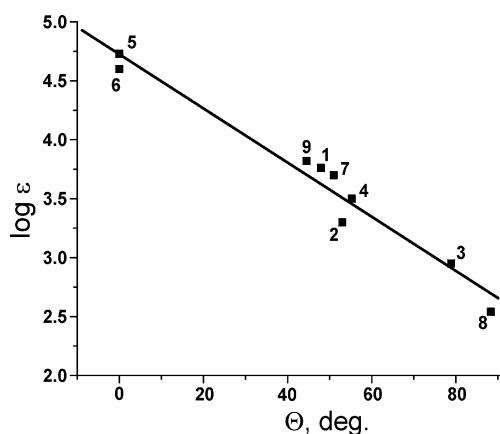
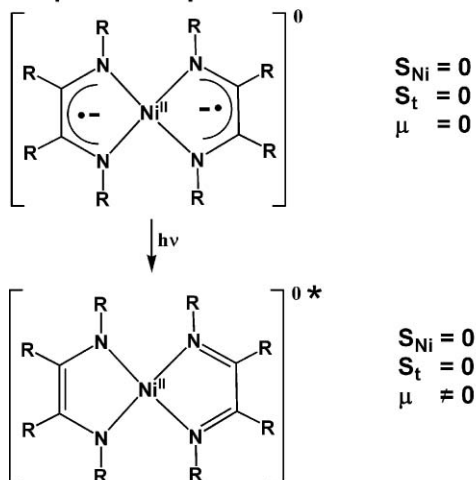
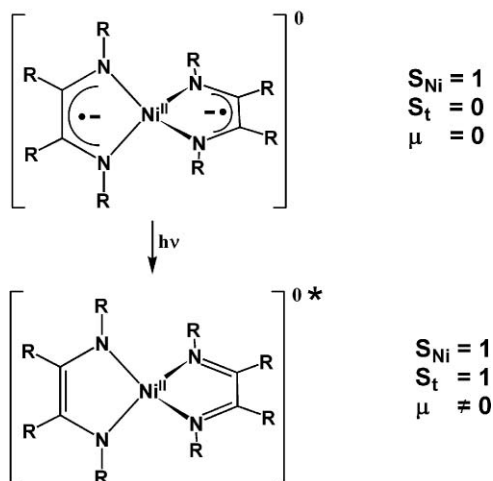


Fig. 4 Plot of the intensity ($\log \epsilon$) of the lowest energy transition of $[\text{Ni}^{\text{II}}(\text{L}')_2]^0$ complexes vs. the dihedral angle θ of the two metallacycles Ni–N–C–C–N. The numbers refer to the complex numbers listed in Table 2.

LLCT in square planar $[\text{Ni}^{\text{II}}(\text{L}')_2]^0$ is spin- and dipole allowed



LLCT in tetrahedral $[\text{Ni}^{\text{II}}(\text{L}')_2]^0$ is spin-forbidden but dipole allowed



Scheme 2 LLCT transitions of square planar and tetrahedral $[\text{Ni}(\text{L}')_2]$ complexes.

they are shown in Fig. 5. In contrast to the two EPR spectra⁶ of the two geometrical isomers of $[\text{Ni}^{\text{I}}(^3\text{L}^{\text{Ox}})_2]^+$ the spectra of $[\text{Ni}^{\text{I}}(^1\text{L}^{\text{Ox}})_2]^+$ and $[\text{Ni}^{\text{I}}(^2\text{L}^{\text{Ox}})_2]^+$ each consist only of one component.

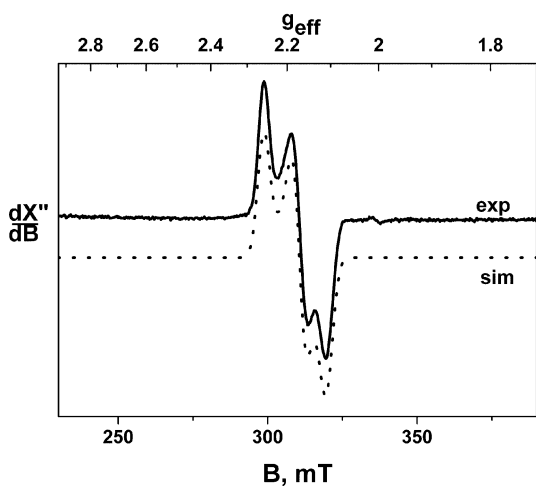
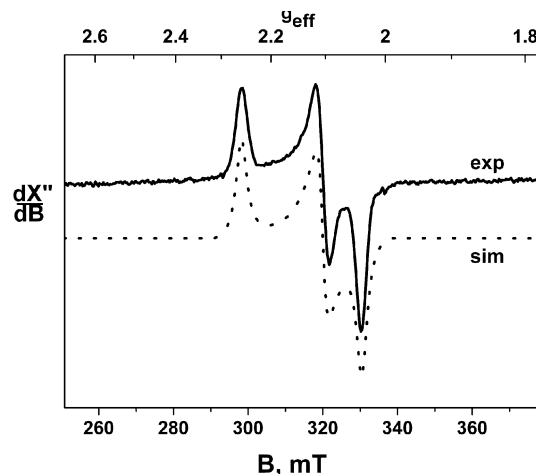


Fig. 5 X-Band EPR spectra of **2** (CH_2Cl_2 –toluene 1 : 1 v/v) at 30 K (top) and **4** (CH_2Cl_2) at 10 K (bottom). Conditions for **2** (and **4**): frequency: 9.43 (9.43) GHz; power 1.26 (25.2) μW ; modulation 7 (10) G. See Table 3 for simulation parameters.

Table 3 summarizes the observed and calculated values. In all three cases the observed g anisotropy of the paramagnetic monocations is quite large indicating that the unpaired electron resides predominantly in a metal d -orbital. Given that the structure of tetrahedral $[\text{Ni}^{\text{I}}(^3\text{L}^{\text{Ox}})_2](\text{PF}_6)$ has been determined⁶ and the oxidation level of the two ligands has been clearly identified as $(^1\text{L}^{\text{Ox}})^0$, we conclude that the monocations **2** and **4** have a very

Table 3 X-Band EPR spectral data of complexes

Complex	g_x		g_y		g_z	
	Exp.	Calcd	Exp.	Calcd	Exp.	Calcd
$[\text{Ni}^{\text{I}}(^3\text{L}^{\text{Ox}})_2]^+$ ^a	2.066	2.085	2.210	2.244	2.444	2.370
	2.070		2.198		2.359	
$[\text{Ni}^{\text{I}}(^1\text{L}^{\text{Ox}})_2]^+$	2.038	2.067	2.105	2.182	2.259	2.271
$[\text{Ni}^{\text{I}}(^2\text{L}^{\text{Ox}})_2]^+$	2.109	2.095	2.171	2.181	2.258	2.307

^a Ref. 6.

Table 4 Crystallographic data for **1**, **3**-hexane, and **5**

	1	3 -hexane	5
Formula	C ₃₀ H ₄₄ N ₄ Ni	C ₆₀ H ₈₀ N ₄ Ni	C ₁₉ H ₂₂ I ₂ N ₂ Ni
<i>M</i>	615.48	926.07	590.90
Space group	<i>P</i> $\bar{1}$, No. 2	<i>P</i> $\bar{1}$, No. 2	<i>P</i> $\bar{1}$, No. 2
<i>a</i> /Å	11.3674(8)	13.1901(6)	7.0556(6)
<i>b</i> /Å	11.8340(8)	13.8920(6)	8.2305(6)
<i>c</i> /Å	13.8385(8)	14.9786(6)	18.0170(12)
<i>a</i> /°	65.052(5)	93.853(3)	94.370(4)
<i>β</i> /°	80.316(5)	93.563(3)	98.977(4)
<i>γ</i> /°	77.999(5)	94.205(3)	98.200(4)
<i>V</i> /Å ³	1644.2(2)	2724.8(2)	1017.69(13)
<i>Z</i>	2	2	2
<i>T</i> /K	100(2)	100(2)	100(2)
ρ_{calcd} /g cm ⁻³	1.243	1.129	1.928
Refl. collected, $2\theta_{\text{max}}$ /°	42057, 60.00	35076, 50.00	7093/, 44.98
Unique refl., <i>R</i> (int), <i>I</i> > 2σ(<i>I</i>)	9582, 0.045, 7568	9590, 0.064, 7841	2161, 0.117, 1577
No. of params, restr.	398, 0	626, 18	112, 0
λ /Å, μ (Kα)/cm ⁻¹	0.71073, 6.22	0.71073, /3.96	0.71073, 39.90
<i>R</i> 1 ^a , goodness of fit ^b	0.0427, 1.022	0.0607, 1.095	0.0806, 1.083
<i>wR</i> 2 ^c (<i>I</i> > 2σ(<i>I</i>))	0.0926	0.1183	0.1688
Residual density/e Å ⁻³	+0.44, -0.23	+0.53, -0.34	+1.21, -1.59

^a Observation criterion: $I > 2\sigma(I)$. $R1 = \sum \|F_o\| - |F_c| / \sum \|F_o\|$. ^b GooF = $[\sum [w(F_o^2 - F_c^2)^2] / (n - p)]^{1/2}$. ^c $wR2 = [\sum [w(F_o^2 - F_c^2)^2] / \sum [w(F_o^2)^2]]^{1/2}$ where $w = 1/\sigma^2(F_o^2) + (aP)^2 + bP$, $P = (F_o^2 + 2F_c^2)/3$.

similar electronic structure with a central Ni(II) (d⁸; *S* = 1/2) ion. As discussed previously⁶ a [Ni^{II}(L^{Ox})(L[•])]⁺ ↔ [Ni^{II}(L[•])(L^{Ox})]⁺ charge distribution has been ruled out (see below).

Crystal structures

The crystal structures of the neutral complexes **1**, **3**-hexane, and **5** have been determined by single crystal X-ray crystallography at 100(2) K. Table 4 gives crystallographic data, and Tables 5 and 6 summarize important bond lengths in **1**, **3**-hexane, and **5**, respectively.

As noted before^{5,6} and shown in Scheme 1, the oxidation level of a given, N,N'-coordinated α-diimine derivative such as the enediimide(2-), (L^{Red})²⁻, the π radical monoanion, (L[•])¹⁻, or the neutral α-diimine, (L^{Ox})⁰, can be clearly identified from the observed C–N and C–C bond lengths. The average C–NR distance at ~1.29 Å is indicative of C=N double bonds in M(L^{Ox}) fragments, or of a C–N bond order of ~1.5 in M(L[•]) fragments at 1.34 Å, or of a C–N single bond in M(L^{Red}) fragments at ~1.40 Å.

Table 6 Selected experimental and calculated bond distances (Å) in **5**

	Expt.	Calcd
Ni–N1	1.996(16)	2.077
Ni–N4	2.008(14)	2.080
Ni–I2	2.471(3)	2.564
Ni–I1	2.542(3)	2.578
N1–C1	1.28(2)	1.281
C2–C3	1.46(3)	1.470
C3–N4	1.30(2)	1.290

Fig. 6 displays the structure of a neutral, tetrahedral molecule in **5**. The average C–NR bond length at 1.29 Å and the C–C bond distance at 1.46 Å are typical for a neutral (L^{Ox})⁰ oxidation level.

Fig. 7 and 8 exhibit the structure of the neutral molecules in crystals of **1** and **3**-hexane, respectively. In both structures the two ligands are equivalent and in both cases the average C–N and C–C bond lengths are compatible only with the (L[•])¹⁻ oxidation level. Thus, **1** and **3**-hexane each contain a central Ni(II) ion and two ligand π radical monoanions. It is noted that the average Ni–N

Table 5 Selected experimental bond distances (Å) in **1** and **3**. Calculated values are from BS(2,2) *M*_S = 0 B3LYP DFT calculations

	Expt. (1)	Calcd (1)	Calcd (2)	Expt. (3)	Calcd (3)	Calcd (4)
Ni–N1	1.948(1)	2.060	2.095	1.963(2)	2.046	2.144
Ni–N4	1.921(1)	2.032	2.086	1.999(2)	2.140	2.212
Ni–N31	1.948(1)	2.046	2.088	1.967(2)	2.046	2.159
Ni–N34	1.928(1)	2.043	2.093	1.978(2)	2.141	2.191
N1–C2	1.337(2)	1.325	1.297	1.327(2)	1.339	1.292
C2–C3	1.405(3)	1.420	1.474	1.402(4)	1.419	1.476
C3–N4	1.330(2)	1.324	1.288	1.326(2)	1.322	1.280
N31–C32	1.338(2)	1.336	1.297	1.340(2)	1.340	1.294
C32–C33	1.397(2)	1.420	1.474	1.396(2)	1.418	1.474
C33–N34	1.330(2)	1.324	1.288	1.326(3)	1.323	1.281
θ ^a /°	47.9	47.0	38	53	52	46

^a Dihedral angle between two chelate rings.

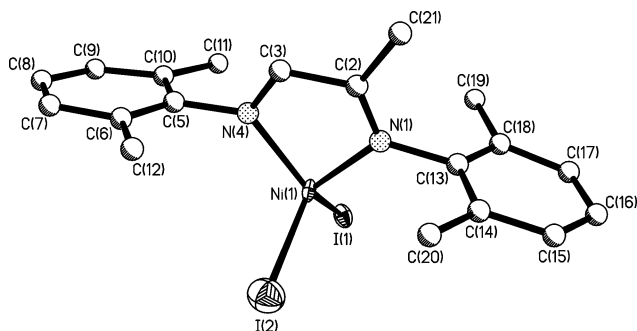


Fig. 6 Structure of the neutral complex in crystals of **5**.

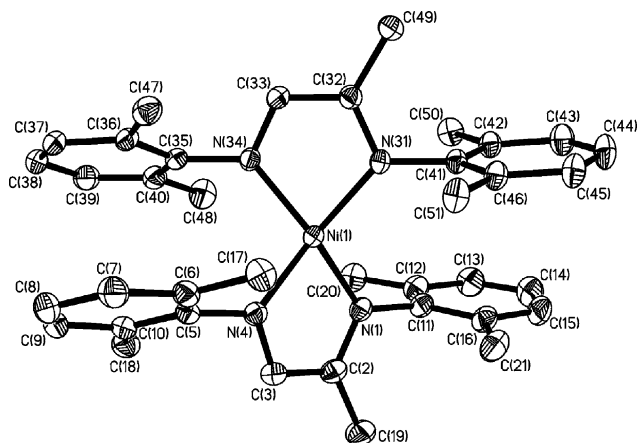


Fig. 7 Structure of the neutral complex in crystals of **1**.

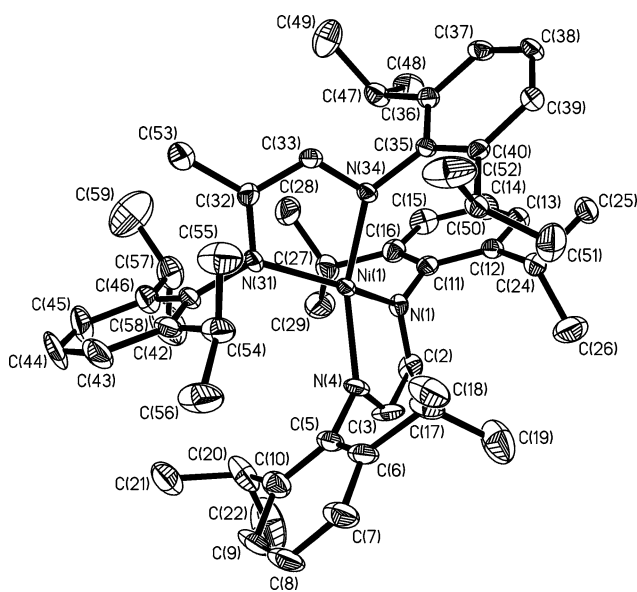


Fig. 8 Structure of the neutral, transoid majority component in crystals of **3**; that of the cisoid minority component is not shown.

bond length in **1** at $1.936 \pm 0.003 \text{ \AA}$ is significantly shorter than in **3**-hexane at $1.977 \pm 0.006 \text{ \AA}$. This is a clear indication that the greater steric bulk of the four isopropyl groups in **2** as compared to four methyl groups in **1** has a significant effect on the overall structure.

The dihedral angle θ between the two five-membered chelate rings Ni–N–C–N in **1** at 48° and in **3**-hexane at 53° indicate that both structures are intermediate between square planar ($\theta = 0$) and regular tetrahedral ($\theta = 90^\circ$).

It is now interesting that solid **3**-hexane consists of two isomers namely the transoid form **A** ($\sim 70\%$) and the cisoid form **B** ($\sim 30\%$). Both forms co-crystallize and lead to an apparent statistical disorder of the 2-methyl group of the ligand backbone. The same ratio has been observed to prevail in solution by ^1H NMR spectroscopy. The proton signal of the 2-methyl groups of the transoid form **A** is observed at -3.62 ppm ($\sim 70\%$) and at -3.27 ($\sim 30\%$) for the cisoid form **B**. From the fact that these signals (and their ratio) is independent of the temperature we conclude that the **A** and **B** forms are not in a dynamic equilibrium in solution. The steric bulky isopropyl groups obviously prevent the interconversion of these two forms.

DFT Calculations

a. Optimized geometries for 1–5. Here, a detailed picture of the molecular and electronic structures of the neutral complexes **1**, **3**, and **5** and of the monocations in **2** and **4** will be developed.

Assuming that tetrahedral **1** and **3** feature a high-spin Ni(II) ion and two ligand radicals, we optimized the ground state geometry for (a) a closed-shell $S = 0$, (b) a high-spin, open-shell $S = 2$, and (c) a BS(2,2) $M_S = 0$ state for **1** and **3**.

For these cases, stationary states on the potential energy surfaces were located. The closed-shell solutions and the $S = 2$ configurations were found to be higher in energy than the BS solutions by 11 and 14 kcal mol $^{-1}$, respectively. An attempt to calculate a BS(1,1) state corresponding to $[\text{Ni}^{\text{I}}(\text{L}^{\cdot})(\text{L}^{\text{ox}})]$ failed; the calculation converged back to the BS(2,2) solution. Thus, the BS(2,2) solution involving a high-spin Ni(II) ion antiferromagnetically coupled to two ligand π radicals, $(\text{L}^{\cdot})^{\pm}$, is the preferred one. The calculated bond distances (Table 5) of the BS solutions within the two equivalent ligands are in acceptable agreement with experiment and support the presence of two $(\text{L}^{\cdot})^{\pm}$ π radicals in both cases. The experimental average Ni–N distance in **1** at $1.936 \pm 0.003 \text{ \AA}$ and in **3** at $1.977 \pm 0.006 \text{ \AA}$ are overestimated by 0.11 and 0.12 \AA , respectively; a result which is typical for the B3LYP functional. It is noteworthy, that the BS calculated dihedral angles between the two five-membered chelate rings in **1** and **3** are in excellent agreement with experiment (Table 5).

For complexes **2** and **4** the open-shell $S = 1/2$ and the BS(2,1) $M_S = 1/2$ states converged to the same solution. Thus, attempts to calculate $[\text{Ni}^{\text{II}}(\text{L}^{\cdot})(\text{L}^{\text{ox}})]^{\pm}$ with a high-spin Ni(II) ion and a single antiferromagnetically coupled ligand π radical reverted to the $S = 1/2$ (Ni(II), d^9) solution. Both ligands in **2** and **4** are identical and the C–N and C–C bond lengths indicate the presence of two neutral $(\text{L}^{\text{ox}})^0$ ligands. These distances agree very well with those found experimentally in $[\text{Ni}^{\text{II}}(\text{L}^{\text{ox}})_2](\text{PF}_6)$.⁶ Significantly, the same ligand distances have been found experimentally and calculated for a spin-unrestricted $S = 1$ state for complex **5**. Thus, the ligands have unambiguously the oxidation level $(\text{L}^{\text{ox}})^0$ (Table 4) in **2**, **4**, and **5**.

b. Electronic structures of 1–5. For pseudo-tetrahedral **5** the MO bonding scheme (supporting information) clearly demonstrates the presence of a central Ni(II) ion since the five highest energy orbitals are of predominantly metal-d character; three of which are doubly occupied and two (originating from the t_2 set)

are singly occupied as is expected for a Ni(II) ion in a tetrahedral ligand field. The Mulliken spin population analysis corroborates this notion where ~ 1.6 electrons are located at the central Ni(II) ion and 0.25 on both iodide ligands but only 0.08 on the ligand (L^{ox})⁰.

A qualitative MO bonding scheme derived from the spin-unrestricted BS(2,2) calculation for **1** is shown in Fig. 9. Five orbitals which are predominantly of metal-d character are again identified. Three of these are found in the spin-up and spin-down manifolds; they are doubly occupied. The other two nickel-based orbitals originating from the t_2 set occur only in the spin-up manifold. These two orbitals are thus singly occupied with

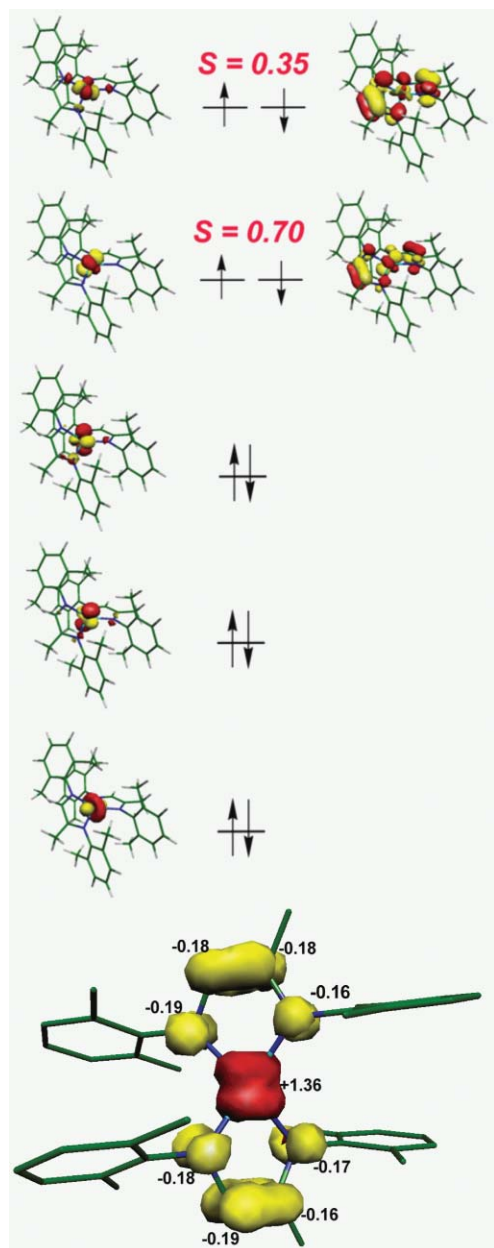


Fig. 9 Qualitative MO scheme of the corresponding orbitals of magnetic pairs and metal-d orbitals of **1** as derived from the broken symmetry DFT calculations (B3LYP) (top). Spin density plot of **1** together with approximate values of the spin density of the Mulliken spin population analysis (bottom). Hydrogen atoms are omitted for clarity.

parallel spins. This pattern defines a high-spin Ni(II) configuration at the metal center. In addition, two ligand centered orbitals are identified in the spin-down manifold which are not populated in the spin-up manifold; thus leading to the observed overall $M_S = 0$ BS state. These orbitals correspond to two symmetry-adapted combinations of the SOMO of the two ligand radicals. Complex **1**, therefore, features a high-spin Ni(II) ion which is strongly antiferromagnetically coupled to two ligand-centered π radicals.

As pointed out previously, the spin density arising from BS SCF (DF or HF) calculations is unphysical. Nevertheless, it is quite suggestive of the physical situation at hand. The spin density plot shown in Fig. 9 (bottom) nicely shows the antiparallel spin alignment between the high-spin Ni(II) (positive spin density in red) and the radical ligands (negative spin density in yellow).

An approximate breakdown of the spin density into atomic contributions *via* a spin population analysis supports the presence of two unpaired electrons at the nickel ion with a positive spin and two unpaired electrons with a negative spin localized on the two ligand π radicals.

The corresponding orbital transformation can be used to visualize the overlapping magnetic pairs of the system. The spin-orbitals obtained from single-point unrestricted calculations were transformed in such a way that for each spin-up orbital there exists at most one spin-down partner that has non-zero spatial overlap. Values of S close to 1 indicate a standard doubly occupied MO with little spin-polarization, whereas $S \ll 1$ is the signature of non-orthogonal magnetic orbital pairs. For **1**, two such magnetically interacting pairs which interact *via* a π pathway have been identified. Each of these pairs consists of one metal orbital and the corresponding ligand radical orbital. The mutual overlap between those two orbitals are 0.35 and 0.70, as shown in Fig. 9. This indicates fairly strong antiferromagnetic interactions between the two metal and two ligand radicals.

Exactly the same situation has previously been described by us for similar tetrahedral nickel complexes containing *o*-diiminobenzosemiquinonate(1⁻)⁷ and *S*-methylisothiosemicarbazionate(1⁻)¹¹ π radicals. Similar calculations for **3** afford exactly the same picture (see ESI).

The calculated electronic structure of the monocation in **2** is shown in Fig. 10. Five predominantly metal-d orbitals are clearly identified; the first four of which are doubly occupied whereas the fifth d-orbital is only singly occupied. This is indicative of the presence of a Ni(I) ion (d^9 ; $S_{\text{Ni}} = 1/2$). All ligand orbitals are either doubly or not occupied at all as is expected for two closed-shell, diamagnetic (L^{ox})⁰ ligands. The Mulliken spin population analysis shows that the unpaired electron (+1.04) is localized at the metal-center and no spin density is observed on the ligands. For the monocation in **4** (see ESI) the same picture has been obtained.

Finally, we have calculated reasonable g -tensors for the monocations in **2** and **4** by using the above DFT methodology (Table 3). The experimental and calculated g_x , g_y , g_z values are in good agreement. The large g -anisotropy is in excellent agreement with the notion that a paramagnetic Ni(I) ion is present in **2** and **4**.

Conclusion

The present work suggests that the electronic structures of the diamagnetic neutral complexes **1** and **3** containing NiN_4 polyhedra which are intermediate between square planar and tetrahedral ($\theta \approx$

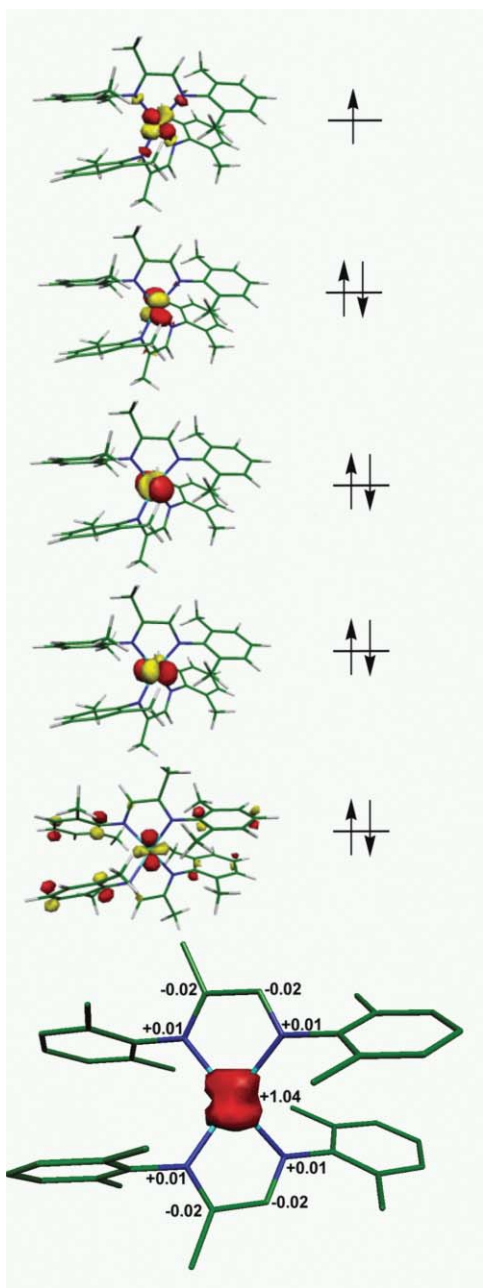


Fig. 10 Qualitative MO scheme of the monocation in **2** as derived from the spin unrestricted $S = 1/2$ DFT calculations (B3LYP) (top). Spin density plot of **2** together with approximate values of the spin density of the Mulliken spin population analysis. Hydrogen atoms are omitted for clarity (bottom).

45°) and other more regular tetrahedral species⁶ ($\theta \approx 90^\circ$) differ slightly (see the respective electronic spectra and the intensities of the LLCT bands). On the other hand, the intriguing redox chemistry remains the same: the monocations are Ni(I) species ($S = 1/2$) with two neutral (L^0) ligands irrespective of the dihedral angle between the two five-membered chelate rings. It is gratifying that broken symmetry DFT calculations of the neutral species clearly indicate that two monoanionic ligand π radicals are present irrespective of θ . In square planar complexes of this type spins strongly couple antiferromagnetically with each other whereas in

the tetrahedral species strong antiferromagnetic coupling to the central nickel(II) ($S_{Ni} = 1$) prevails and a diamagnetic ground state $S = 0$ is attained in both cases.

Experimental

Preparations of compounds

All air-sensitive materials were manipulated under argon using standard Schlenk line procedures or a glovebox. Cyclododecatriene-nickel(0), Ni(cdt), and ferrocenium hexafluorophosphate were used as starting materials. The ligands 2-methyl-1,4-bis(2,6-dimethylphenyl)-1,4-diaza-1,3-butadiene and 2-methyl-1,4-bis(2,6-diisopropylphenyl)-1,4-diaza-1,3-butadiene²⁸ were synthesized according to published procedures.

[Ni^{II}(¹L[•])₂] (1). To a solution of 2-methyl-1,4-bis(2,6-dimethylphenyl)-1,4-diaza-1,3-butadiene (2.390 g, 8.58 mmol) in diethyl ether (10 mL) under an argon blanketing atmosphere was added a solution of Ni(cdt) (1 g, 4.29 mmol) in diethyl ether (20 mL). The resulting red solution was stirred over night at room temperature. The solvent was removed by evaporation under reduced pressure to give a dark red precipitate which was washed with acetonitrile and dried *in vacuo* to yield 2.10 mg of **1** (79%). X-Ray quality crystals were obtained by slow evaporation of the solvent from a concentrated solution of **1** in *n*-hexane. Anal. calcd for C₃₈H₄₄N₄Ni: C, 74.2; H, 7.2; N, 9.1; Ni, 9.5. Found: C, 73.8; H, 7.7; N, 8.7; Ni, 9.1%. ¹H NMR (400 MHz, toluene-*d*₈): δ (ppm) = -1.68 (s, 6H, NCCH₃), 2.06 (s, 12H, C₆H₃CH₃), 2.17 (s, 12H, C₆H₃CH₃), 6.78 (m, 4H, C₆H₃), 6.92 (m, 4H, C₆H₃), 7.03 (m, 4H, C₆H₃), 8.40 (s, 2H, NCH). ¹³C NMR (400 MHz, toluene-*d*₈): δ = 18.48 (CH₃, C₆H₃Me), 19.57 (CH₃, C₆H₃Me), 21.49 (CH₃, NCMe), 124.29 (CH, C₆H₃), 124.39 (CH, C₆H₃), 127.74 (CH, C₆H₃), 128.09 (CH, C₆H₃), 128.45 (CH, C₆H₃), 137.30 (CH, NCH), 143.37 (Cq, NCMe), 157 (Cq, C₆H₃), 160 (Cq, C₆H₃).

[Ni^{II}(¹L^{ox})₂](PF₆) (2). To a solution of **1** (200 mg, 0.32 mmol) in CH₂Cl₂ (10 mL) was added ferrocenium hexafluorophosphate (100 mg, 0.32 mmol) with stirring for 1.5 h at 20 °C. The dark red colour of the solution immediately turned to dark violet. The resulting solution was filtered and the filtrate was concentrated to ~1 mL by evaporation of the solvent under reduced pressure. *n*-Hexane (10 mL) was added and the resulting suspension was stirred for 1 h. A dark violet precipitate formed, which was isolated by filtration, washed with *n*-hexane (2 × 5 mL) and dried *in vacuo* to give 0.21 g of **2** (87%). MS (ESI, pos. ion, CH₂Cl₂), m/z = 614 {**2** - PF₆}⁺. Anal. calcd for C₃₈H₄₄N₄F₆NiP: C, 60.0; H, 5.8; N, 7.4; F, 15.0; Ni, 7.7; P, 4.1. Found: C, 60.2; H, 5.8; N, 7.3; F, 15.2; Ni, 7.7; P, 4.0%.

[Ni^{II}(²L[•])₂]*n*-hexane (3-*n*-hexane). To a pale yellow solution of 2-methyl-1,4-bis(2,6-diisopropylphenyl)-1,4-diaza-1,3-butadiene (3.53 g, 9.06 mmol) in *n*-hexane (30 mL) under an argon blanketing atmosphere was added a solution of Ni(cdt) (1 g, 4.53 mmol) in diethyl ether (20 mL). The resulting violet solution was stirred over night at room temperature. The solvent was removed by evaporation under reduced pressure to give a dark violet precipitate which was washed with acetonitrile and dried *in vacuo* to yield 3.10 g of **3** (81%). X-Ray quality crystals of **3-*n*-hexane** were obtained by cooling a concentrated *n*-hexane solution of **3** to -40 °C. Anal. calcd for crystalline C₆₀H₉₀N₄Ni: C,

77.8; H, 9.8; N, 6.0; Ni, 6.3. Found: C, 77.8; H, 9.4; N, 6.1; Ni, 6.3%. ¹H NMR (400 MHz, toluene-*d*₆): δ (ppm) = −3.62, −3.27 (s, NCCCH₃), 0.4–1.67 (m, C₆H₃(CH(CH₃)₂)₂), 2.50–5.80 (m, C₆H₃(CH(CH₃)₂)₂), 6.83–7.16 (m, C₆H₃), 9.56, 9.61 (s, NCH).

[Ni^{II}(¹L^{ox})₂](PF₆) (**4**). To a solution of **3** (400 mg, 0.476 mmol) in CH₂Cl₂ (10 mL) was added ferrocenium hexafluorophosphate (150 mg, 0.476 mmol) with stirring for 1.5 h at 20 °C. The dark red colour of the solution immediately turned to green. The resulting solution was filtered and the filtrate was concentrated to ~1 mL by evaporation of the solvent under reduced pressure. *n*-Hexane (10 mL) was added and the resulting suspension was stirred for 1 h. A dark violet precipitate was formed, washed with *n*-hexane (2 × 5 mL) and dried *in vacuo* to give 0.40 g of **4** (87%). Anal. calcd for C₅₄H₇₆N₄F₆NiP: C, 65.9; H, 7.8; N, 5.7; F, 11.6; Ni, 6.0; P, 3.1. Found: C, 65.6; H, 7.7; N, 5.6; F, 11.6; Ni, 5.8; P, 3.2%.

[Ni^{II}(¹L^{ox})₂I₂] (**5**). To a solution of NiI₂ (0.94 mg, 3.02 mmol) in tetrahydrofuran (10 mL) under an argon blanketing atmosphere was added a solution of 2-methyl-1,4-bis(2,6-dimethylphenyl)-1,4-diaza-1,3-butadiene (0.84 g, 3.02 mmol) in tetrahydrofuran (6 mL). The resulting red solution was stirred over night at room temperature. The solvent was removed by evaporation under reduced pressure to give a red precipitate which was washed with *n*-hexane and dried *in vacuo* to yield 2.22 mg of **5** (89%). X-Ray quality crystals were obtained by slow evaporation of the solvent from a concentrated solution of **5** in dichloromethane. Anal. calcd for C₁₉H₂₂N₂I₂Ni: C, 36.6; H, 3.8; N, 4.7; I, 43.0; Ni, 9.9. Found: C, 36.4; H, 3.6; N, 4.5; I, 43.0; Ni, 10.0%.

X-Ray crystallographic data collection and refinement of the structures

Dark red single crystals of **1** and **5**, and a red crystal of **3**-hexane were coated with perfluoropolyether, picked up with nylon loops and were mounted in the nitrogen cold stream of the diffractometer. A Bruker-Nonius Kappa-CCD diffractometer equipped with a Mo-target rotating-anode X-ray source and a graphite monochromator (Mo-Kα, λ = 0.71073 Å) was used. Final cell constants were obtained from least squares fits of all measured reflections. Intensity data were corrected for absorption using intensities of redundant reflections.

The structures were readily solved by Patterson methods and subsequent difference Fourier techniques. The Siemens ShelXTL²⁶ software package was used for solution and artwork of the structure, ShelXL97²⁷ was used for the refinement. All non-hydrogen atoms in **1** and **3**-hexane were refined anisotropically but due to the low data quality of **5** only the nickel and iodine atoms were anisotropically refined. Hydrogen atoms were placed at calculated positions and refined as riding atoms with isotropic displacement parameters. Crystallographic data for the compounds are listed in Table 4.

Due to co-crystallization of the two geometrical isomers in **3**-hexane, the methyl group (C23) was found to be statically disordered over two sites. A split atom model with equal thermal displacement parameters of corresponding atoms and restrained bond distances using the EADP and SAME instruction of ShelXL97,²⁷ refined to an occupation ratio of about 72 : 28. The hexane solvent molecule was found to be disordered and was split on two positions in a 68 : 32 ratio using EADP and SAME.²⁷

Crystals of **5** were found to be extremely thin and were weakly diffracting. Due to problems during data integration, reflection data are only complete to about 81%. Only heavy atoms were anisotropically refined since the data/parameter ratio and data quality did not allow full anisotropic refinement.

Acknowledgements

We thank the *Fonds der Chemischen Industrie* for financial support of this work. Heike Schucht is thanked for skilful help with the X-ray data collection.

References

- 1 A. L. Balch and R. H. Holm, *J. Am. Chem. Soc.*, 1966, **88**, 5201.
- 2 (a) H. tom Dieck, M. Svoboda and J. Kopf, *Z. Naturforsch., B: Anorg. Chem., Org. Chem.*, 1978, **33**, 1381; (b) M. Svoboda, H. tom Dieck, C. Krüger and Y.-H. Tsay, *Z. Naturforsch., B: Anorg. Chem., Org. Chem.*, 1981, **36**, 814; (c) H. tom Dieck, M. Svoboda and T. Greiser, *Z. Naturforsch., B: Anorg. Chem., Org. Chem.*, 1981, **36**, 823.
- 3 D. Walther, *Z. Anorg. Allg. Chem.*, 1974, **405**, 8.
- 4 (a) H. Görls, D. Walther and J. Sieler, *Cryst. Res. Technol.*, 1987, **22**, 1145; (b) W. Bonrath, K. R. Pörschke, R. Mynott and C. Krüger, *Z. Naturforsch., B: Chem. Sci.*, 1990, **45**, 1647.
- 5 M. M. Khusniyarov, K. Harms, O. Burhaus and J. Sundermeyer, *Eur. J. Inorg. Chem.*, 2006, 2985.
- 6 N. Muresan, K. Chlopek, T. Weyhermüller, F. Neese and K. Wieghardt, *Inorg. Chem.*, 2007, **46**, 5327.
- 7 K. Chlopek, E. Bothe, F. Neese, T. Weyhermüller and K. Wieghardt, *Inorg. Chem.*, 2006, **45**, 6298.
- 8 P. Ghosh, E. Bill, T. Weyhermüller, F. Neese and K. Wieghardt, *J. Am. Chem. Soc.*, 2003, **125**, 1293.
- 9 (a) D. Herebian, E. Bothe, F. Neese, T. Weyhermüller and K. Wieghardt, *J. Am. Chem. Soc.*, 2003, **125**, 9116; (b) D. Herebian, K. E. Wieghardt and F. Neese, *J. Am. Chem. Soc.*, 2003, **125**, 10997.
- 10 P. C. Searvas, D. J. Stufkens and A. Oskam, *Inorg. Chem.*, 1989, **28**, 1774.
- 11 S. Blanchard, F. Neese, E. Bothe, E. Bill, T. Weyhermüller and K. Wieghardt, *Inorg. Chem.*, 2005, **44**, 3636.
- 12 G. van Koten and K. Vrieze, *Adv. Organomet. Chem.*, 1982, **21**, 151.
- 13 S. Richter, C. Daul and A. von Zelewsky, *Inorg. Chem.*, 1976, **15**, 943.
- 14 C. Corvaja and L. Pasimeni, *Chem. Phys. Lett.*, 1976, 261.
- 15 F. G. N. Cloke, G. R. Hanson, M. J. Henderson, P. B. Hitchcock and C. L. Raston, *J. Chem. Soc., Chem. Commun.*, 1989, 100.
- 16 F. G. N. Cloke, C. I. Dalby, M. J. Henderson, P. B. Hitchcock, C. H. L. Kennard, R. N. Lamb and C. L. Raston, *J. Chem. Soc., Chem. Commun.*, 1990, 1394.
- 17 K.-H. Thiele, V. Lorenz, G. Thiele, P. Zönnchen and J. Scholz, *Angew. Chem., Int. Ed. Engl.*, 1994, **33**, 1372.
- 18 M. G. Gardiner, G. R. Hanson, M. J. Henderson, F. C. Lee and C. L. Raston, *Inorg. Chem.*, 1994, **33**, 2456.
- 19 E. Rijnberg, B. Richter, K.-H. Thiele, J. Boersma, N. Veldman, A. L. Spek and G. van Koten, *Inorg. Chem.*, 1998, **37**, 56.
- 20 T. Pott, P. Jutz, B. Neumann and H.-G. Stämmler, *Organometallics*, 2001, **20**, 1965.
- 21 R. J. Baker, R. D. Farley, C. Jones, D. P. Mills, M. Kloth and D. M. Murphy, *Chem.–Eur. J.*, 2005, **11**, 2972.
- 22 T. Pott, P. Jutz, W. Kaim, W. W. Schoeller, B. Neumann, A. Stämmler, H.-G. Stämmler and M. Wanner, *Organometallics*, 2002, **21**, 3169.
- 23 (a) R. J. Baker, R. D. Farley, C. Jones, M. Kloth and D. M. Murphy, *Chem. Commun.*, 2002, 1196; (b) R. J. Baker, R. D. Farley, C. Jones, M. Kloth and D. M. Murphy, *J. Chem. Soc., Dalton Trans.*, 2002, 3844.
- 24 H. M. Tuononen and A. F. Armstrong, *Dalton Trans.*, 2006, 1885.
- 25 H. M. Tuononen and A. F. Armstrong, *Inorg. Chem.*, 2005, **44**, 8277.
- 26 *ShelXTL V.5*, Siemens Analytical X-Ray Instruments Inc., Madison, WI, USA, 1994.
- 27 G. M. Sheldrick, *ShelXL97*, University of Göttingen, Germany, 1997.
- 28 N. O. Druzhkov, I. A. Teplova, V. N. Glushakova, N. A. Skorodumova, G. A. Abakumov, B. Zhao, E. Berluche, D. N. Schulz, L. S. Baugh, C. A. Ballinger, K. R. Squire, J.-A. M. Canich and M. P. Bubnov, *Patent PCT/US2003/022356, WO2004/007509*, 2004.